NANO LETTERS
Cite This: Nano Lett. 2019, 19, 8103−8108
Letter
pubs.acs.org/NanoLett

# Direct Visualization of Independent Ta Centers Supported on Two-Dimensional $TiO_2$ Nanosheets

Zhenyu Bo,[†] Nicholas E. Thornburg,[‡] Lingxuan Peng,[†] Jose Julio Gutierrez Moreno,[§] Michael Nolan,[§] Laurence D. Marks,[†] and Justin M. Notestein*[,‡]

[†]Department of Materials Science and Engineering, Northwestern University, Evanston, Illinois 60208, United States
[‡]Department of Chemical and Biological Engineering, Northwestern University, Evanston, Illinois 60208, United States
[§]Tyndall National Institute, University College Cork, Lee Maltings, Dyke Parade, Cork T12R5CP, Ireland

Supporting Information

**ABSTRACT:** Highly dispersed, supported oxides are ubiquitous solid catalysts but can be challenging to characterize with atomic precision. Here, it is shown that crystalline anatase $TiO_2$ nanosheets (~5 nm thick) are ideal supports for imaging highly dispersed active sites. Ta cations were deposited by several routes, and high-resolution high angle annular dark-field scanning transmission electron microscopy was used to determine the location of Ta with respect to the $TiO_2$ lattice and quantify Ta−Ta distances. In the best case, it is shown that >80% of Ta atoms are isolated from one another, whereas other techniques are blind to this critical catalytic property or give only qualitative estimates. $TiO_2$ nanosheets may prove to be a useful platform for other types of catalysis studies.

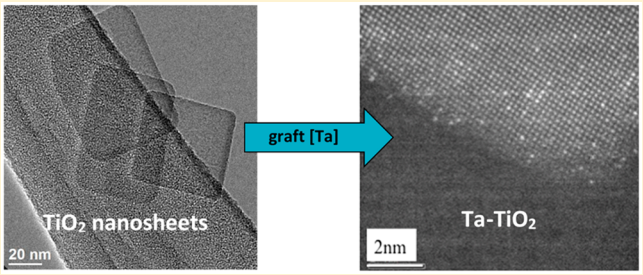


**KEYWORDS:** *HAADF STEM, supported catalysts, oxides, microscopy, single atom catalysts*

Heterogeneous catalysts are solid materials that catalyze reactions in the gas or liquid phase and are essential in chemicals manufacturing, fuels production, and emissions control.[1,2] They take a variety of forms, including supported metal nanoparticles such as $Pt/Al_2O_3$ for hydrogenation/dehydrogenation or combustion,[3] bulk oxides such as the complex MoVTeNbO materials used in ammoxidation,[4] or supported metal oxides such as $TiO_x/SiO_2$ and $VO_X/TiO_2$.[5,6] This last category is frequently used in reactions such as the selective oxidation of alcohols and alkenes, emissions control, and photocatalysis.[7−10]

The reactivity of any heterogeneous catalyst is dependent on the number of the active atoms (e.g., Ti atoms in $TiO_X/SiO_2$ catalysts) that are accessible to the reactants.[6,11,12] To keep this value as high as possible, catalysts are typically synthesized to be as dispersed as possible while retaining their active form, giving oxide domains that are ideally present as single cations on the support, small clusters, or monolayers. In addition, supported oxides are also well-known to be "structure-sensitive", in that their precise atomic connectivity to other active atoms and to the support has a large impact on catalytic rates and selectivities.[13−16]

Therefore, the catalysis community is continuously looking for methods to control the chemical environment and the dispersion of active sites during the synthesis of supported metal oxide catalysts. These methods can include the use of bulky or well-defined precursors to enforce site-isolation,[17,18] multinuclear precursors to create small clusters,[19−21] thermolytic molecular precursors,[22,23] substituted silsesquioxanes,[23,24] atomic layer deposition,[25−27] and engineered supports,[28−30] among many other approaches.

Beyond the synthesis, a significant challenge in supported oxides of all types is characterizing them with atomic precision. Historically, characterization of the active sites of supported oxide catalysts has been via probe reactions and via X-ray absorption, UV−visible, NMR, vibrational, and other spectroscopies. However, these techniques all give local properties of the probed atom and are also averaged over the whole sample, making it challenging to tease out some of the finer details of synthesis structure−function relationships such as the distribution of atoms across a surface. Finally, chemical site counting methods can provide distributions of the properties of active sites[31,32] but do not necessarily provide structural information.

Significant advances have been made in recent years for the direct, atomic-level visualization of supported catalyst active sites by electron microscopy, even as the active sites themselves trend toward single-atom dimensions.[33,34] However, there remain several significant limitations. First, most imaging of single-atom and small cluster catalysts has occurred

Received: August 12, 2019
Revised: October 17, 2019
Published: October 29, 2019





DOI: 10.1021/acs.nanolett.9b03305
Nano Lett. 2019, 19, 8103−8108

**Scheme 1. Modification of Anatase 001-Terminated $TiO_2$ Nanosheets ($nsTiO_2$) with Ta and with an $Al_2O_3$ Overcoat**

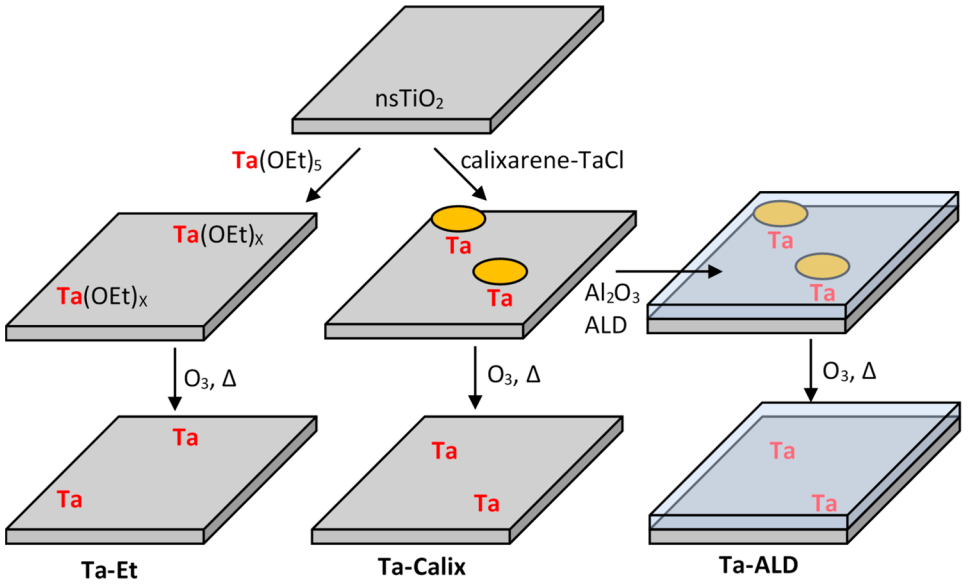


with third row, low-valent, late transition metals (e.g., Au, Pt, Ir).[33−35] These elements provide good Z-contrast and are widely used catalysts. In contrast, supported, high-valent, early transition metal cations and oxides have not been the target of these types of imaging studies, likely because the first row elements are more commonly used in catalysis within these groups. Second, zeolites and other crystalline oxides like $SrTiO_3$ have been preferred for atomic-resolution imaging of supported species, in part because of the relative ease of imaging along a particle edge on such supports.[36,37] It is more challenging to image species with atomic resolution on the surface of traditional, high surface area supports such as $Al_2O_3$, $TiO_2$, and $SiO_2$ because of their amorphous or highly faceted surfaces and relatively large primary particles. There have been successes using core−shell or very small support oxide particles to image and locate single catalyst atoms,[38,39] but it remains very challenging to focus highly converged electron beams on more than a small area at a time.

In this letter, we report the use of 2D $TiO_2$ nanosheets ($nsTiO_2$) as nearly ideal support materials for the direct visualization of highly dispersed catalysts across large particle surface areas. Here, we demonstrate its utility for tantalum oxides ($TaO_X/TiO_2$) to address the dearth of imaging of supported, high-valent, early transition metal cations, but these supports should be generally applicable for imaging supported catalysts. The use of thin (∼5 nm), flat, anatase $TiO_2$ nanosheets instead of traditional oxide particles makes it possible to keep the entire surface in focus during high-resolution high angle annular dark-field (HAADF) imaging, rather than very small regions on a particle edge, as is typical for conventional supports. Moreover, in contrast to prior examples of scanning transmission electron microscopy (STEM),[40] scanning tunneling spectroscopy (STM),[41,42] or atom-probe tomography,[43] high surface area powders are used here, permitting bulk characterization tools to be used on the same material with no special modifications. Second- and third-row highly dispersed metal oxides are less commonly used than their first-row counterparts but have recently gained attention for having comparable, or in many cases greater, activity or selectivity in a variety of thermochemical transformations.[7,15] TaOx-based materials have been shown to be interesting in a variety of selective oxidation reactions,[44−46] and Ta-$TiO_2$ specifically is of interest as an acid catalyst[47] and for its photocatalytic properties.[48−50]

The images collected here provide direct evidence for single-atom dispersion and provide the distribution of Ta−Ta nearest-neighbor distances over a wide area, giving insight into the sensitivity of the TaOx structure on the Ta precursor used for synthesis. It also gives insight into the effects of postsynthetic modifications such as subsequent atomic layer deposition of an additional oxide. Precursor and postsynthesis modification have both been shown to strongly influence the catalyst activity and stability,[25,30,51] but as mentioned above, direct connections to surface speciation have remained elusive.

$TiO_2$ nanosheets ($nsTiO_2$) were synthesized using titanium butoxide and hydrofluoric acid under autoclave conditions following previously reported procedures.[52] The $N_2$ physisorption specific surface area measured (Supporting Information Figure S1) by the Brunauer−Emmett−Teller method is 145 $m^2/g$. These materials consist of platelets with particle dimensions of length and width below 100 nm and thickness below 10 nm (Figure S2) Typical particles have length and width of ∼60 nm and a thickness of ∼5 nm. These materials have pure anatase phase with X-ray diffraction peaks corresponding to the (101), (004), (200), (105), and (211) crystal planes (Figure S3).[53] The particles are not annealed, and the large faces are unreconstructed and [001]-terminated.[52] The particles are flat for imaging over extended distances, but the faces are not atomically smooth and are expected to contain the types of surface defects found in other $TiO_2$ materials.

To deposit Ta atoms, (illustrated in Scheme 1), $nsTiO_2$ was dispersed in a toluene solution containing either calixarene-TaCl (30 mM, 40 mL, ultimately giving material **Ta-Calix**)[54] as a representative bulky precursor previously shown to help enforce site-isolation on silica or $Ta(OEt)_5$ (Sigma-Aldrich, 15 mM, 10 mL, ultimately giving materials **Ta-Et**), and the solution was heated to reflux for 24 h. The modified $nsTiO_2$ was washed with anhydrous toluene and dried under dynamic vacuum at room temperature. This procedure grafts the Ta



DOI: 10.1021/acs.nanolett.9b03305
Nano Lett. 2019, 19, 8103−8108

atoms at a surface density of ~0.3 Ta $nm^{-2}$, or 70 $\mu$mol Ta $g^{-1}$ as determined by thermogravimetric analysis (to measure calixarene ligand content, Figure S4) and ICP-OES (Ta content). This loading was chosen because it is approximately the geometrical limit resulting from the large calixarene ligand.[25] Some samples of as-synthesized **Ta-Calix** were coated with <1 nm $Al_2O_3$ using atomic layer deposition (ALD) of five alternating cycles of $Al(CH_3)_3$ and $H_2O$,[25] ultimately leading to material **Ta-ALD**. Finally, all samples were treated in flowing $O_3$ at 110 °C to remove any residual organic ligands. In addition to electron microscopy, samples were also characterized by X-ray diffraction (XRD) and X-ray photoelectron (XPS), diffuse reflectance UV−visible (DRUV−vis), and Raman spectroscopies. See the Supporting Information for full procedures.

HAADF imaging was completed using a JEOL JEM-ARM200CF aberration-corrected scanning transmission electron microscope. To prepare the sample for imaging, ethanol suspensions of samples were drop-cast onto TEM grids and air-dried. The HAADF images were acquired using a probe of ~0.078 nm, an emission current of 15 $\mu$A, and a beam current of ~19pA with a 40 $\mu$m condenser lens aperture. The collection angle of the HAADF was greater than 80°. Ta atom nearest neighbor distances (NND) were calculated using ImageJ software.

Conventional spectroscopies and other characterization tools are often limited in the information they can provide for mixed or supported oxides as they give ensemble averages of the materials. XRD after Ta deposition or after ALD (Figure S3) shows no changes or additional features. This indicates that neither did a $TaO_x$ crystal phase form on top of the $nsTiO_2$ nor did Ta insert into the $TiO_2$ lattice to any significant extent, but it provides no information on the actual TaOx structure adopted. XPS (Figure S5) shows binding energy peaks at 458.6 and 464.5 eV in the Ti 2p region and at 530.5 eV in the O 1s region, which are typical of $Ti^{4+}$ and oxygen ions in metal oxides.[53] The Ta 4f peaks around 26 and 28 eV confirm the presence of Ta with high oxidation state in the Ta-containing samples.[55−57] The absence of observable features near 855 $cm^{-1}$ in the Raman spectrum could indicate the absence of Ta−O−Ta bonds that would be found in larger clusters.[58] However, as is often the case with supported oxide catalysts, stronger conclusions are precluded by the relatively low loadings of Ta and the strong contribution from $nsTiO_2$ itself. Likewise, DRUV−vis can be a useful tool for characterizing supported oxides[6,7] but here cannot distinguish the Ta-containing materials from the parent $nsTiO_2$ (Figure S7). Overall, XRD, XPS, and Raman studies confirm the presence of small amounts of highly dispersed Ta oxide on anatase $nsTiO_2$ but cannot provide further details.

Therefore, high-resolution HAADF-STEM images were acquired to enable direct observation of the distribution of Ta atoms on the $TiO_2$ surface with atomic resolution. Figure 1a shows the structure of **Ta-Et** taken along the [001] direction of the $nsTiO_2$ crystallite. The image clearly demonstrates that the Ta atoms are located on top of the Ti−O columns, and there were no Ta atoms located between columns. This alignment requires that the Ta atoms were present either directly above the Ti lattice sites or as substitutions for Ti atoms within the lattice or at the surface. Because of the synthesis method and the mild postsynthesis treatments, it is most likely that Ta grafts directly above the Ti atoms. Density functional theory (see the Supporting Information for details) confirms that, regardless of the extents of Ta atom hydration and surface hydroxylation, the stable configuration places Ta atoms directly above a Ti atom column, as illustrated in Figures 1b and c. We note that the Ta atoms occupy different crystallographic positions depending on the state of hydration, although we cannot verify this from the microscopy. The circles in Figure 1a highlight some of the many isolated Ta atoms (no Ta atoms at the neighboring lattice position) in this sample. The squares in Figure 1 show some potential pairs or oligomers of Ta atoms at adjacent sites.

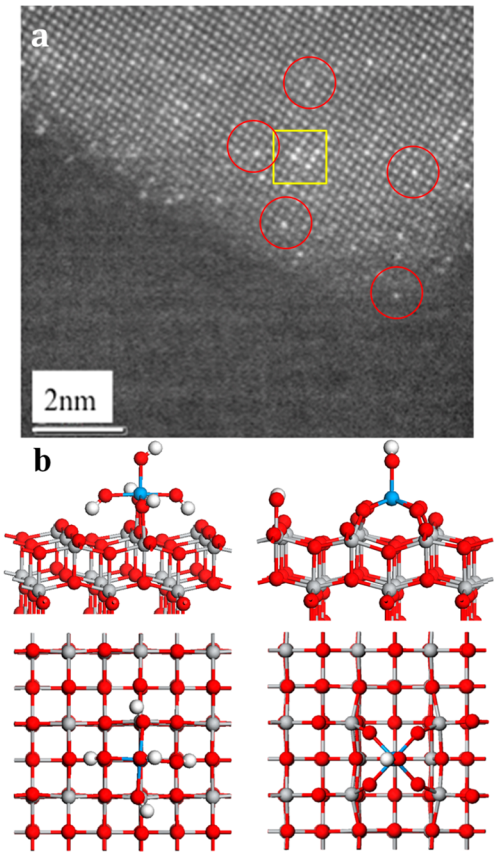


**Figure 1.** (a) High-resolution HAADF-STEM image of sample **Ta-Et** acquired along the [001] direction of the $TiO_2$ support. A median filter with a window of size 2 was applied to this image. The unprocessed image is given in Figure S8. The bright dots are individual Ta toms. Red circles highlight isolated Ta atoms, and the yellow square highlights potential regions where Ta atoms are found in adjacent sites. (b) Optimized structures of $Ta^{5+}$ supported on a $TiO_2$ anatase (001) surface generated using density functional theory modeling showing alignment of Ta with Ti columns, whether fully hydrated (left) or dehydrated (right); see the Supporting Information for discussion. Red = O, gray = Ti, blue = Ta, white = H.

Next, the unique ability to locate Ta atoms over longer distances on $nsTiO_2$ is used to map out Ta−Ta distances for the materials. Figure 2 shows a representative set of atomic resolution HAADF-STEM images of **Ta-Et**, **Ta-Calix**, and **Ta-ALD** taken in plan-view to obtain information about Ta−Ta spacing. Because of the planar supports, single images provide information representative of the entire sample. For example, Figure 2d shows 186 atoms over approximately 350 $nm^2$ of imaged area (700 $nm^2$ of $TiO_2$ surface). This gives 3.7 $nm^2$ $Ta^{1-}$, in good agreement with the specific surface area of the $nsTiO_2$ divided by the total amount of Ta grafted (3.3 $nm^2$ $Ta^{1-}$). From visual inspection alone, the two Ta precursors do



DOI: 10.1021/acs.nanolett.9b03305
Nano Lett. 2019, 19, 8103−8108

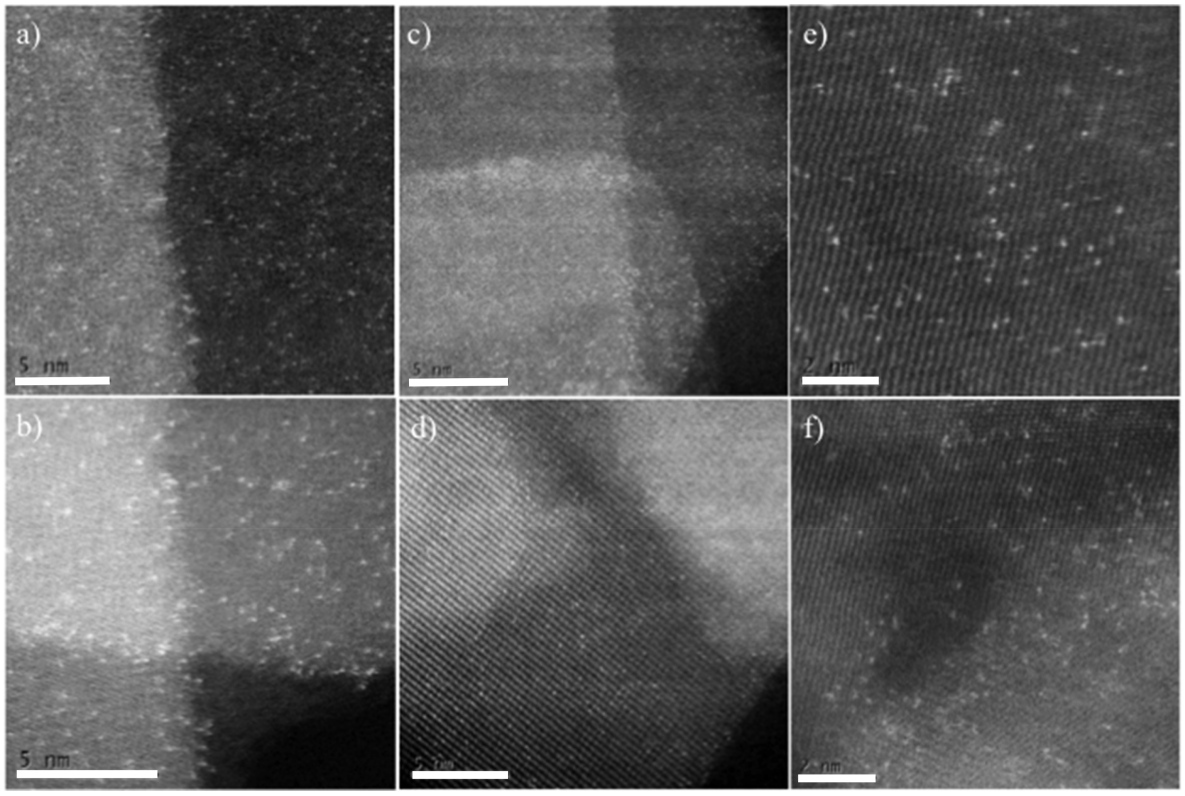


**Figure 2.** Representative high resolution HAADF-STEM images of (a, b) **Ta-Calix**, (c, d) **Ta-Et**, and (e, f) **Ta-ALD**. Scale bars in panels a–d are 5 nm. Scale bars in e and f are 2 nm.

not produce markedly different Ta distributions on the surface with many isolated atoms in both cases. In addition, the Ta distribution is not apparently changed by $Al_2O_3$ overcoating by ALD. The ALD process utilizes the very reactive molecule $Al(CH_3)_3$ and generates water vapor at moderate temperatures, and it was initially suspected that the process might significantly rearrange the surface TaOx. We also note that while the nsTiO$_2$ supports can be damaged by long electron beam exposures, the Ta remain as single atoms, with no obvious changes to their orientation with respect to the TiO$_2$ surface (Figures S9a and b). This contrasts with control materials such as Ta on silica nanospheres, in which the Ta is challenging to visualize initially then obviously aggregates during microscopy (Figures S9c and d).

These images enabled by the extended, flat surface of nsTiO$_2$ allows for statistically meaningful estimates ($N$ = 134–186 Ta atoms) of the distribution of supported Ta atoms from a small number of images. The observed NND are calculated for all visible Ta atoms in Figure 2 (see also Figure S10). The median NND for materials **Ta-Et**, **Ta-Calix**, and **Ta-ALD** are 0.5, 0.7, and 0.5 nm, respectively. From the 3.3 nm$^2$ Ta$^{1-}$ average loading, Ta perfectly dispersed on the surface would have an apparent Ta–Ta separation of 0.9 nm. We also quantitatively estimate the fraction of Ta atoms that are "isolated" from another by placing a cutoff Ta–Ta separation of >0.4 nm from the nearest neighbor, approximately the Ta–O–Ta distance in $Ta_2O_5$.[59] The cumulative frequency distributions in Figure 3 show that for all materials, >60% of Ta atoms are isolated from each other with potentially >80% of the Ta atoms being isolated in the case of **Ta-Calix**, which is derived from the bulky precursor. It is emphasized that these estimates are conservative. Because the imaging technique

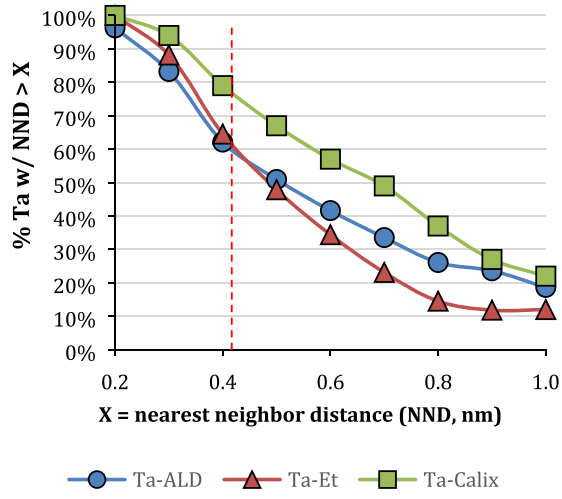


**Figure 3.** Cumulative frequency plot of NND (Ta to Ta distance in nanometers) for samples **Ta-Et** (186 atoms counted), **Ta-Calix** (134 atoms counted), and **Ta-ALD** (161 atoms counted). Ta to Ta distances ≤0.4 nm, indicated by the red line, might indicate the formation of Ta–O–Ta bonds.

visualizes all Ta atoms in a 2D space, Ta atoms sitting on the other side of the TiO$_2$ nanosheets were also imaged, thus increasing the apparent Ta surface density.

"Isolated" sites have long been argued from spectroscopy to be the most active sites in a number of reactions,[35,60] and many synthetic methods, including the use of bulky ligands such as calixarene,[54,25] have been specifically developed to bias the system toward a preponderance of these sites. For the first time, we have directly demonstrated the validity of these claims



DOI: 10.1021/acs.nanolett.9b03305
Nano Lett. 2019, 19, 8103–8108

from HAADF-STEM imaging. Recalling that **Ta-ALD** is derived from the same precursor material as **Ta-Calix**, the full analysis of the Ta−Ta distances also shows that the conditions of the ALD indeed cause some rearrangement and aggregation of TaOx, even if the aggregation is not severe enough to be observed by bulk techniques. In conclusion, we have demonstrated the use of $TiO_2$ nanosheets as excellent 2D supports for high resolution STEM imaging of highly dispersed, supported catalysts and quantification of atom−atom distance distributions. We are currently working to apply this technique to other catalytic metals and systems.

## ■ ASSOCIATED CONTENT

### Supporting Information

The Supporting Information is available free of charge on the ACS Publications website at DOI: 10.1021/acs.nanolett.9b03305.

Materials synthesis procedures; characterization, including $N_2$ physisorption, XRD, TGA, XPS, Raman, UV−visible; additional TEM and Ta−Ta distance histograms; computational details; and results (PDF)

## ■ AUTHOR INFORMATION


### Corresponding Author

*E-mail: j-notestein@northwestern.edu.

### ORCID

Michael Nolan: 0000-0002-5224-8580

Justin M. Notestein: 0000-0003-1780-7356


### Notes

The authors declare no competing financial interest.

## ■ ACKNOWLEDGMENTS

This material is based upon work supported by the U.S. Department of Energy, Office of Science, Office of Basic Energy Science, under Award DOE DE-FG02-03ER15457 to the Institute for Catalysis for Energy Processes (ICEP) at Northwestern University. This work was supported by the Materials Research Center (MRSEC) at Northwestern University with Grant DMR-112126. N.E.T. and J.M.N. acknowledge financial support from the Dow Chemical Company. This work made use of the EPIC facility of the NUANCE Center at Northwestern University, which has received support from the Soft and Hybrid Nanotechnology Experimental (SHyNE) Resource (NSF NNCI-1542205); the MRSEC program (NSF DMR-112126) at the Materials Research Center; the International Institute for Nanotechnology (IIN); the Keck Foundation; and the State of Illinois, through the IIN. This work made use of the JEOL JEM-ARM200CF in the Electron Microscopy Service [Research Resources Center, University of Illinois at Chicago (UIC)]. J.J.G.M. and M.N. acknowledge support from the Irish Environmental Protection Agency UisceSense project (W-2015-MS-21) and the SFI-NSF-DEL US Ireland R&D Partnership Program, Grant SFI US/14/e2915 and access to computational resources through the Irish Center for High End Computing. We acknowledge supply of raw materials ($TiO_2$ nanosheets) by Dr. Kevin Schwartzenberg (Northwestern University) and atomic layer deposition work by Cassie George (Northwestern University).

## ■ REFERENCES


(1) Satterfield, C. N. *Heterogeneous Catalysis in Industrial Practice*, 2nd ed.; McGraw Hill: New York, NY, 1991.
(2) Mizuno, N.; Misono, M. *Chem. Rev.* **1998**, *98*, 199−218.
(3) Stanislaus, A.; Cooper, B. H. *Catal. Rev.: Sci. Eng.* **1994**, *36*, 75−123.
(4) Millet, J.; Roussel, H.; Pigamo, A.; Dubois, J.; Jumas, J. *Appl. Catal., A* **2002**, *232*, 77−92.
(5) Olthof, B.; Khodakov, A.; Bell, A. T.; Iglesia, E. J. *J. Phys. Chem. B* **2000**, *104*, 1516−1528.
(6) Gao, X.; Wachs, I. E. *Catal. Today* **1999**, *51*, 233−254.
(7) Thornburg, N. E.; Thompson, A. B.; Notestein, J. M. *ACS Catal.* **2015**, *5*, 5077−5088.
(8) Wachs, I. E. *Dalton Trans* **2013**, *42*, 11762−11769.
(9) Mallat, T.; Baiker, A. *Chem. Rev.* **2004**, *104*, 3037−3058.
(10) Clerici, M.; Bellussi, G.; Romano, U. *J. Catal.* **1991**, *129*, 159−167.
(11) Xu, Z.; Xiao, F.-S.; Purnell, S.; Alexeev, O.; Kawi, S.; Deutsch, S.; Gates, B. *Nature* **1994**, *372*, 346−348.
(12) Van Santen, R. A. *Acc. Chem. Res.* **2009**, *42*, 57−66.
(13) Weckhuysen, B. M.; Keller, D. E. *Catal. Today* **2003**, *78*, 25−46.
(14) Grant, J. T.; Carrero, C. A.; Love, A. M.; Verel, R.; Hermans, I. *ACS Catal.* **2015**, *5*, 5787−5793.
(15) Onfroy, T.; Clet, G.; Houalla, M. *J. Phys. Chem. B* **2005**, *109*, 14588−14594.
(16) Tian, H.; Ross, E. I.; Wachs, I. E. *J. Phys. Chem. B* **2006**, *110*, 9593−9600.
(17) Prieto-Centurion, D.; Notestein, J. M. *J. Catal.* **2011**, *279*, 103−110.
(18) Jarupatrakorn, J.; Tilley, T. D. *J. Am. Chem. Soc.* **2002**, *124*, 8380−8388.
(19) Wegener, S. L.; Marks, T. J.; Stair, P. C. *Acc. Chem. Res.* **2012**, *45*, 206−214.
(20) Wegener, S. L.; Kim, H.; Marks, T. J.; Stair, P. C. *J. Phys. Chem. Lett.* **2011**, *2*, 170−175.
(21) Hess, C.; Hoefelmeyer, J. D.; Tilley, T. D. *J. Phys. Chem. B* **2004**, *108*, 9703−9709.
(22) Fujdala, K. L.; Tilley, T. D. *J. Catal.* **2003**, *216*, 265−275.
(23) Nozaki, C.; Lugmair, C. G.; Bell, A. T.; Tilley, T. D. *J. Am. Chem. Soc.* **2002**, *124*, 13194−13203.
(24) Duchateau, R. *Chem. Rev.* **2002**, *102*, 3525−3542.
(25) Canlas, C. P.; Lu, J.; Ray, N. A.; Grosso-Giordano, N. A.; Lee, S.; Elam, J. W.; Winans, R. E.; Van Duyne, R. P.; Stair, P. C.; Notestein, J. M. *Nat. Chem.* **2012**, *4*, 1030−6.
(26) Liu, R.; Lin, Y.; Chou, L. Y.; Sheehan, S. W.; He, W.; Zhang, F.; Hou, H. J.; Wang, D. *Angew. Chem.* **2011**, *123*, 519−522.
(27) Herrera, J. E.; Kwak, J. H.; Hu, J. Z.; Wang, Y.; Peden, C. H. *Top. Catal.* **2006**, *39*, 245−255.
(28) Thomas, J. M.; Hernandez-Garrido, J. C.; Raja, R.; Bell, R. G. *Phys. Chem. Chem. Phys.* **2009**, *11*, 2799−2825.
(29) Chal, R.; Gérardin, C.; Bulut, M.; Van Donk, S. *ChemCatChem* **2011**, *3*, 67−81.
(30) Gao, X.; Wachs, I. E. *Top. Catal.* **2002**, *18*, 243−250.
(31) Eaton, T. R.; Boston, A. M.; Thompson, A. B.; Gray, K. A.; Notestein, J. M. *ChemCatChem* **2014**, *6*, 3215−3222.
(32) Eaton, T. R.; Campos, M. P.; Gray, K. A.; Notestein, J. M. *J. Catal.* **2014**, *309*, 156−165.
(33) Ding, K.; Gulec, A.; Johnson, A. M.; Schweitzer, N. M.; Stucky, G. D.; Marks, L. D.; Stair, P. C. *Science* **2015**, *350*, 189−192.
(34) Fu, Q.; Saltsburg, H.; Flytzani-Stephanopoulos, M. *Science* **2003**, *301*, 935−938.
(35) Kistler, J. D.; Chotigkrai, N.; Xu, P.; Enderle, B.; Praserthdam, P.; Chen, C. Y.; Browning, N. D.; Gates, B. C. *Angew. Chem.* **2014**, *126*, 9050−9053.
(36) Flytzani-Stephanopoulos, M.; Gates, B. C. *Annu. Rev. Chem. Biomol. Eng.* **2012**, *3*, 545−574.
(37) Chen, B.-R.; Crosby, L. A.; George, C.; Kennedy, R. M.; Schweitzer, N. M.; Wen, J.; Van Duyne, R. P.; Stair, P. C.;




DOI: 10.1021/acs.nanolett.9b03305
*Nano Lett.* 2019, 19, 8103−8108

Poeppelmeier, K. R.; Marks, L. D.; Bedzyk, M. J. *ACS Catal.* **2018**, *8*, 4751−4760.
(38) DeRita, L.; Resasco, J.; Dai, S.; Boubnov, A.; Thang, H. V.; Hoffman, A. S.; Ro, I.; Graham, G. W.; Bare, S. R.; Pacchioni, G.; Pan, X.; Christopher, P. *Nat. Mater.* **2019**, *18*, 746−751.
(39) Lee, B.-H.; Park, S.; Kim, M.; Sinha, A. K.; Lee, S. C.; Jung, E.; Chang, W. J.; Lee, K.-S.; Kim, J. H.; Cho, S.-P.; Kim, H.; Nam, K. T.; Hyeon, T. *Nat. Mater.* **2019**, *18*, 620−626.
(40) Chang, T.-Y.; Tanaka, Y.; Ishikawa, R.; Toyoura, K.; Matsunaga, K.; Ikuhara, Y.; Shibata, N. *Nano Lett.* **2014**, *14*, 134−138.
(41) Fernandez-Garcia, M.; Martinez-Arias, A.; Hanson, J.; Rodriguez, J. *Chem. Rev.* **2004**, *104*, 4063−4104.
(42) Bell, A. T. *Science* **2003**, *299*, 1688−1691.
(43) Buurmans, I. L.; Weckhuysen, B. M. *Nat. Chem.* **2012**, *4*, 873−886.
(44) Morlanes, N.; Notestein, J. M. *J. Catal.* **2010**, *275*, 191−201.
(45) Nauert, S. L.; Savereide, L.; Notestein, J. M. *ACS Catal.* **2018**, *8*, 7598−7607.
(46) Avenier, P.; Taoufik, M.; Lesage, A.; Solans-Monfort, X.; Baudouin, A.; de Mallmann, A.; Veyre, L.; Basset, J. M.; Eisenstein, O.; Emsley, L.; Quadrelli, E. A. *Science* **2007**, *317*, 1056−1060.
(47) Chen, Y. S.; Fierro, J. L. G.; Tanaka, T.; Wachs, I. E. *J. Phys. Chem. B* **2003**, *107*, 5243−5250.
(48) Visinescu, C. M.; Sanjines, R.; Lévy, F.; Marcu, V.; Pârvulescu, V. I. *J. Photochem. Photobiol., A* **2005**, *174* (2), 106−112.
(49) Baiju, K. V.; Shajesh, P.; Wunderlich, W.; Mukundan, P.; Kumar, S. R.; Warrier, K. G. K. *J. Mol. Catal. A: Chem.* **2007**, *276* (1), 41−46.
(50) Feng, X.; Shankar, K.; Paulose, M.; Grimes, C. A. *Angew. Chem., Int. Ed.* **2009**, *48* (43), 8095−8098.
(51) Iglesia, E. *Appl. Catal., A* **1997**, *161* (1−2), 59−78.
(52) Liang, Y. T.; Vijayan, B. K.; Lyandres, O.; Gray, K. A.; Hersam, M. C. *J. Phys. Chem. Lett.* **2012**, *3* (13), 1760−1765.
(53) Södergren, S.; Siegbahn, H.; Rensmo, H.; Lindström, H.; Hagfeldt, A.; Lindquist, S.-E. *J. Phys. Chem. B* **1997**, *101* (16), 3087−3090.
(54) Morlanés, N.; Notestein, J. M. *J. Catal.* **2010**, *275* (2), 191−201.
(55) Masuda, Y.; Wakamatsu, S.; Koumoto, K. *J. Eur. Ceram. Soc.* **2004**, *24* (2), 301−307.
(56) Liu, J.; Yang, H.; Tan, W.; Zhou, X.; Lin, Y. *Electrochim. Acta* **2010**, *56* (1), 396−400.
(57) Liu, X.; Wu, X.; Scott, K. *Catal. Sci. Technol.* **2014**, *4* (11), 3891−3898.
(58) Chen, Y.; Fierro, J. L.; Tanaka, T.; Wachs, I. E. *J. Phys. Chem. B* **2003**, *107* (22), 5243−5250.
(59) Takahara, Y.; Kondo, J. N.; Takata, T.; Lu, D.; Domen, K. *Chem. Mater.* **2001**, *13* (4), 1194−1199.
(60) Yang, M.; Allard, L. F.; Flytzani-Stephanopoulos, M. *J. Am. Chem. Soc.* **2013**, *135* (10), 3768−3771.



DOI: 10.1021/acs.nanolett.9b03305
*Nano Lett.* 2019, 19, 8103−8108